HHS Public Access

Author manuscript

Nanomedicine. Author manuscript; available in PMC 2017 April 01.

Published in final edited form as:

Nanomedicine. 2016 April ; 12(3): 655–664. doi:10.1016/j.nano.2015.10.012.

Development of Exosome-encapsulated Paclitaxel to Overcome MDR in Cancer cells

Myung Soo Kim[1,2], **Matthew J. Haney**[1,2], **Yuling Zhao**[1,2], **Vivek Mahajan**[1,2], **Irina Deygen**[3], **Natalia L. Klyachko**[1,2,3], **Eli Inskoe**[2], **Aleksandr Piroyan**[1,2], **Marina Sokolsky**[1,2], **Onyi Okolie**[2], **Shawn D. Hingtgen**[1,2], **Alexander V. Kabanov**[1,2,3], and **Elena V. Batrakova**[1,2,*]

[1]Center for Nanotechnology in Drug Delivery, University of North Carolina at Chapel Hill, Chapel Hill, North Carolina, USA

[2]Eshelman School of Pharmacy, University of North Carolina at Chapel Hill, Chapel Hill, North Carolina, USA

[3]Deparment of Chemical Enzymology, Faculty of Chemistry, M.V. Lomonosov Moscow State University, Moscow, Russia

Abstract

Exosomes have recently come into focus as “natural nanoparticles” for use as drug delivery vehicles. Our objective was to assess the feasibility of an exosome-based drug delivery platform for a potent chemotherapeutic agent, paclitaxel (PTX), to treat MDR cancer. Herein, we developed and compared different methods of loading exosomes released by macrophages with PTX (exoPTX), and characterized their size, stability, drug release, and *in vitro* antitumor efficacy. Reformation of the exosomal membrane upon sonication resulted in high loading efficiency and sustained drug release. Importantly, incorporation of PTX into exosomes increased cytotoxicity more than 50 times in drug resistant $MDCK_{MDR1}$ (Pgp+) cells. Next, our studies demonstrated a nearly complete co-localization of airway-delivered exosomes with cancer cells in a model of murine Lewis Lung Carcinoma pulmonary metastases, and a potent anticancer effect in this mouse model. We conclude that exoPTX holds significant potential for the delivery of various chemotherapeutics to treat drug resistant cancers.

Graphical abstract

Exosomes released by autologous macrophages were loaded with paclitaxel (PTX) upon ultrasound treatment. The obtained formulation (exoPTX) showed a high loading capacity, sustained drug release, profound ability to accumulate in resistant cancer cells, and increased cytotoxicity compared to PTX *in vitro* and *in vivo*.

*Correspondence should be addressed to E.V.B. (batrakov@email.unc.edu) UNC Eshelman School of Pharmacy, University of North Carolina at Chapel Hill, Chapel Hill, NC 27599-7362, Phone: 919-537-3712, batrakov@email.unc.edu.

No competing interests are present.

Keywords

cancer; drug resistance; exosome; paclitaxel; Pgp

BACKGROUND

The recently emerged field of nanotechnology holds great promise for developing drug delivery systems with targeting and controlled-release characteristics for cancer treatment; there have been many new advances and innovations made in this field during the past decade (1). A large proportion of chemotherapeutic drugs have low aqueous solubility, consequently requiring the use of specialized delivery vehicles (liposome, polymeric nanoparticles, *etc.*) for parenteral administration. Regrettably, many of these synthetic drug delivery vehicles cause severe side effects, including organ toxicity and/or immune response.

Another factor that considerably limits the efficacy of chemotherapeutics is multiple drug resistance (MDR), which may be intrinsic or acquired (2, 3), and is mediated by different mechanisms, in particular, the overexpression of the drug efflux transporter P-glycoprotein (Pgp). As a result, the response rate following treatment remains very low for many types of malignancies, including, malignant gliomas, metastatic breast cancer, *etc.* (2-4). To date, there has been limited success in overcoming drug resistance in cancers through the use of novel small molecule chemotherapeutics (5, 6), or nanoformulations of existing chemotherapeutics (7-9). These efforts did result in improved patient outcomes; however, the non-specific inhibition of Pgp frequently increased drug toxicity due to alteration of drug elimination pathways in the liver, kidney, *etc*. (10).

Exosomes are membrane-derived vesicles ~40 - 200 nm in diameter (11) that can be found in extracellular bodily fluids (*e.g*. urine, saliva, cerebrospinal fluid) and in conditioned cell culture media (12). They are formed in multivesicular bodies (MVB) inside the cells (5, 12). Exosomes naturally function as intercellular messengers, carrying RNA and proteins (13). Recently, exosomes have begun to be explored for use as drug delivery vehicles for nucleic acids (14-19), gene delivery (20), and small molecule drugs, such as curcumin (12, 21, 22), and doxorubicin (23). It was demonstrated that exosomes have the exceptional ability to interact with cellular membranes, and deliver their payload to target cells (24, 25). Several studies indicate that exosomes may have a specific cell tropism, according to their characteristics and origin, which can be used to target them to disease tissues and/or organs (26). Furthermore, collected from patients' tissues or blood-born immunocytes, allogenic exosomes may have an immune privileged status, which allows for decreased drug clearance and immune responce compared to PEGylated nanoformulations (27). Thus, exosomes may function as an "invisibility cloak" for incorporated therapeutic agents, diminishing clearance

by the mononuclear phagocyte system and concurrently increasing drug transport to target tissues. Thus, exosomes may comprise advantages of both synthetic nanocarriers and cell-mediated drug delivery, avoiding the rapid clearance and toxicity associated with synthetic vehicles, as well as the complexity in utilizing cell-mediated drug delivery systems in clinic. These unique features make exosomes an attractive option for use as a drug delivery vehicle for cancer treatment.

Herein, we have developed a new exosome-based formulation of PTX, a commonly used chemotherapeutic agent. The main objectives of this study were: (i) prepare and characterize a new formulation of exosomes loaded with PTX (exoPTX), (ii) assess the feasibility of using exoPTX for MDR-related anticancer therapy, and (iii) identify mechanisms underlying the effects of exoPTX in MDR cancer cells. Our results indicate that exosomes may represent a promising novel delivery platform for treatment of MDR neoplasms.

METHODS

Reagents

PTX and Doxorubicin (DOX) was purchased from LC Laboratories (Woburn, MA). Lipophilic fluorescent dyes, 1,1'-dioctadecyl-3,3,3',3'-tetramethylindo-carbocyanine perchlorate (DIL), and 2-decanoyl-1-(*O*-(11-(4,4-difluoro-5,7-dimethyl-4-bora-3a,4a-diaza-*s*-indacene-3-propionyl-amino)undecyl)-*sn*-glycero-3-phosphocholine (BODIPY-PC), were purchased from Invitrogen (Carlsbad, CA,) and Molecular Probes (Eugene, OR), respectively. Rhodamine 123 (R123), 4′,6-diamidino-2-phenylindole dihydrochloride (DAPI), and Triton X-100 were obtained from Sigma-Aldrich (St. Louis, MO,). Cell culture medium and fetal bovine serum (FBS) were purchased from Gibco Life Technologies, (Grand Island, NY). Fluorescent polystyrene nanoparticles (Fluoro-Max G100) were obtained from Thermo Fisher Scientific (Waltham, MA). ExoQuick-TC™ Exosome Precipitation Solution was obtained from System Biosciences (Mountain View, CA).

Cells

RAW 264.7 macrophages, Madin-Darby canine kidney $MDCK_{WT}$ and $MDCK_{MDR1}$ cells were purchased from ATCC (Manassas, VA) and cultured in Dulbecco's modified Eagle's medium (DMEM) high glucose (Gibco) supplemented with 10% FBS, 1% penicillin and streptomycin at 37°C and 5% CO_2. Murine Lewis lung carcinoma cell subline (3LL-M27), a highly metastatic lung clone, was a generous gift from Dr. L. Pelletier (CHUL, Laval University, QC, Canada).

Pgp protein levels in sensitive and resistant cancer cells were determined by western blot as previously reported (28) using monoclonal antibodies to Pgp, C219 (Dako Corp., Carpinteria, CA; at dilution 1:100), and secondary horseradish peroxide donkey anti-mouse IgG antibodies (Amersham Life Sciences, Cleveland, OH; at dilution 1:1500). To correct for loading differences, the Pgp levels were normalized to the constitutively expressed β-actin stained with anti-β-1-chicken integrin (Sigma Chemical Co., at dilution 1:200). Specific bands were visualized using a chemiluminescence kit (Pierce, Rockford, IL).

Characterization of Exosomes

Exosomes were harvested from the conditioned media of RAW 264.7 cells cultured in exosome-depleted media using the ExoQuick-TC™ Kit (System BioSciences; Mountain View, CA) and characterized by Nanoparticle Tracking Analysis (NTA), Dynamic Light Scattering (DLS), Atomic Force Microscopy (AFM) and Western Blot Analysis as described previously (29).

BODIPY-PC was used as a probe to examine the fluidic properties of exosomal membranes as described earlier (30). Briefly, 30 μL exosomes with a concentration of 4×10^{11} particles/mL were mixed with 20 μL BODIPY-PC (0.03 mg/ml) (31) and supplemented with 70 μL deionized water; the mixture was incubated for 45 min at 37°C in the dark. Unbound label was removed using a Zeba^{TM} column (Life Technologies).

Drug Loading into Exosomes

For PTX and DOX loading into exosomes, purified exosomes (~10^{11} exosomes) were first mixed with PTX or DOX in 1 mL PBS. Different methods of drug loading were investigated: incubation at room temperature (RT), electroporation, and sonication. *For the incubation method*, the admixture was incubated at 37°C for 1 hour with shaking. *For the electroporation method*, exosomes were mixed with PTX and added to a chilled 4 mm electroporation cuvette. The mixture was then electroporated using an Eppendorf Eporator (Eppendorf AG, Hamburg, Germany) at 1000 kV for 5 ms, and then incubated at 37°C for 30 min to allow for recovery of the exosomal membrane. *For the sonication method*, the PTX-exosome or DOX-exosome mixture was sonicated using a Model 505 Sonic Dismembrator with .25” tip with the following settings: 20% amplitude, 6 cycles of 30 s on/off for three minutes with a two minute cooling period between each cycle. After sonication, exoPTX or exoDOX solution were incubated at 37°C for 60 min to allow for recovery of the exosomal membrane. Excess free drug was separated from exoPTX or exoDOX by size exclusion chromatography using a NAP-10 Sephadex G25 column (GE Healthcare, Buckinghamshire, UK).

The amount of PTX loaded into exosomes was measured by a high performance liquid chromatography (HPLC) method. Briefly, exoPTX (10^{10} exosomes/0.1mL) in a microcentrifuge tube was placed on a heating block set to 75°C to evaporate solvent. Then, an equal volume of acetonitrile was added and the mixture was vortexed, sonicated and then centrifuged at 13,000 rpm (Thermo Legend Micro 21) for 10 min. Following centrifugation, the supernatant was taken and filtered through a Corning Regenerated Cellulose .2 μm syringe filter and transferred into HPLC autosampler vials. 20 μL aliquots were injected into the HPLC system (Agilent 1200, Agilent Technologies, Palo Alto, CA). All analyses were performed using a C18 column (Supelco Nucleosil C18, 250 mm × 4.6 mm, 5 μm, 100 Å, Sigma-Aldrich,) with a mobile phase of H_2O:acetonitrile (45:55, v/v) at a flow rate of 1 mL/min at 30°C. Absorbance was measured at 227 nm to monitor the elution of PTX.

To measure PTX release, freshly prepared exoPTX were placed in a 300K MWCO Float-A-Lyzer G2 device (Spectrum Laboratories, Houston, TX). The device was then placed in PBS under sink conditions at RT with stirring. Samples were taken at time points from inside the

dialysis tube and were analyzed by HPLC as described above. The amount of PTX released from exoPTX was expressed as a percentage of total PTX and plotted as a function of time.

Accumulation of Exosomes and Exosome-incorporated PTX in Cancer Cells

To quantify the amount of exosomes taken up by cells, exosomes were stained with a lipophilic fluorescent dye, DIL as described previously (29). Then, DIL-labeled exosomes, or fluorescently-labeled liposomes, or polystyrene nanoparticles (NPs, Fluoro-Max G100, Thermo Fisher Scientific), were added in equal numbers (~10^8 particles/well) and incubated with 3LL-M27 cells at 37°C and 5% CO_2 for various times. After each time point, the media was removed and cells were washed 3x with PBS and fixed by incubating with Formal-Fixx (Thermo Fisher Scientific), and examined by confocal microscopy or using a Shimadzu RF5000 fluorescent spectrophotometer. In case of exoPTX or Taxol, drugs were added in equimolar amounts to the $MDCK_{WT}$, or $MDCK_{MDR1}$ cells and incubated for 72h. The cell suspension was then lysed and analyzed for PTX content by HPLC as described above.

In vitro Cytotoxicity Assay

The *in vitro* antitumor efficacy of exoPTX was assessed using a standard MTT (3-(4,5-dimethyl-2-thiazolyl)-2,5-diphenyl-2-H-tetrazoliumbromide) assay with three cancer cell lines, and compared to Taxol as described earlier (32). Briefly, cancer cells (MDCKMDR1, MDCKwt, and 3LL-M27) were seeded at 5,000 cells/well in 100 μL of media in 96-well plates overnight. Various concentrations of exosomes isolated from macrophages conditioned media and loaded with PTX by sonication, or empty sonicated exosomes, or Taxol, or PTX were added to cancer cells for 48 hours at 37C, 5% CO2. Following the incubation, the cells were washed and incubated with MTT reagent as described in (33). The cytotoxic activity of PTX was then evaluated using a standard MTT assay (34). The absorbance at 570nm was measured using a Shimadzu RF5000 fluorescent spectrophotometer. The survival values were determined in relation to control cells cultured in drug-free media. All experiments were repeated at least three times. SEM values were less than 10%.

Production of a Lentiviral Vector (LV) and Transduction of LLC cells

Lentiviral vector encoding a fusion between the optical reporter mCherry (GBM8FlmC, red) and firefly luciferase (FLuc) were created by PCR amplification of the cDNA sequences for mCherry and FLuc from pEmCherry (Clontech) and pcDNA-Luciferase (Addgene) with restriction enzyme sequences that were engineered into the primers. To create the final constructs, mCherry was digested with BamHI/EcoV and FLuc was digested with EcoV/XhoI. The digested fragments were ligated into the BamHI/XhoI digested pTK402 LV transfer vector (a kind gift from Dr. Tal Kafri, The University of North Carolina at Chapel Hill). LV-mCherryFLuc viral vectors were packaged in 3LL-M27 cells by transient transfection using the psPAX2 and pMD2.G (Addgene) packaging plasmids and following previously described protocols (35).

To utilize bioluminescence and fluorescence imaging, 3LL-M27 cells were transduced with lentiviral vectors encoding an mCherry and Renilla luciferase (mC-RL) fusion protein. The viral construct also encoded for a puromycin resistance gene downstream of mCherry which

was introduced to enable for selection of nearly 100% positively transduced cells. A robust expression of both the fluorescent and bioluminescent markers was observed, and no difference in proliferation was detected between modified and unmodified cells. These cells (8FlmC-FLuc-3LL-M27) were used for biodistribution and therapeutic efficacy studies.

Biodistribution of Exosomes in Mice with Pulmonary Metastases

The experiments were performed with female C57BL/6 mice (Charles River Laboratories, Durham, NC) eight weeks of age in strict accordance with the recommendations in the Guide for the Care and Use of Laboratory Animals of the National Institutes of Health. The animals were kept five per cage with an air filter cover under light- (12-hours light/dark cycle) and in a temperature-controlled (22 ± 1° C) environment. All manipulations with the animals were performed under a sterilized laminar hood. Food and water were given *ad libitum*.

C57BL/6 mice (n = 4) were injected intra tail vein (*i.v.*) with 8FlmC-FLuc-3LL-M27 cells (5×10^6 cells/mouse in 100 μL saline) and tumor lung metastases were allowed to establish for 10-12 days. Twelve days following cancer cells *i.v.* injection, DID-labeled exosomes isolated from autologous macrophages were administered intranasally (*i.n.*, 10^7 particles/ 10μl × 2) to mice with lung metastases. Four hours later, mice were sacrificed, perfused, lungs were extracted and sectioned on a microtome at a thickness of 20 μm; nuclei were stained with DAPI (300 mM, 5 min). The images of lung sections were examined by a confocal fluorescence microscopic system ACAS-570 and corresponding filter set, and processed using ImageJ software.

In another experiment, mice with established GBM8FlmC-metastases were injected *i.n.* with non-labeled exosomes loaded with Dox by sonication as described above (10^7 particles/ 10μL × 2). Four hours later mice were sacrificed, perfused; lungs were extracted, sectioned, and co-localization of Dox with pulmonary metastases was visualized by confocal microscopy.

Therapeutic Efficacy of exoPTX against Pulmonary Metastases

The antineoplastic effects of exoPTX were evaluated in a mouse model of pulmonary metastases. For this purpose, C57BL/6 mice were *i.v.* injected with 8FlmC-FLuc-3LL-M27 cancer cells (5×10^6 cells/100 μL/ mouse). Forty eight hours later, mice were treated *i.n.* with exoPTX (10^7 particles/10 μl × 2), or Taxol (50 mg/kg/mouse), or saline as a control (n = 7) every other day with a total of seven treatments. Tumor progression was monitored by luminescence using the IVIS system as described in (36). The animals were imaged at various time points (1 – 22 days) post-treatment as described (36). The chemoluminescent signal was quantified by Living Image® 2.50 software. To assess the amount of cancer metastases at day 22, mice were sacrificed, perfused, and lung slides obtained on microtome (Thermo Scientific) were examined by confocal microscopy.

Statistical Analysis

For the all experiments, data are presented as the mean ± *S.E.M.* Tests for significant differences between the groups were performed using a t-test or one-way ANOVA with

multiple comparisons (Fisher's pairwise comparisons) using GraphPad Prism 5.0 (GraphPad software, San Diego, CA). A minimum *p* value of 0.05 was chosen as the significance level.

RESULTS

Manufacture and characterization of exosomal formulations of PTX (exoPTX)

Exosomes collected from the conditioned media of RAW 264.7 macrophages were characterized by size, charge, protein content, and morphology (**Fig. 1A, B, and D**). Exosomes showed elevated expression of exosome-associated proteins (Alix, TSG101, and Flotillin) as compared to cell lysate, which displayed greater levels of β-actin (**Fig. 1B**). Naïve empty exosomes had a narrow size distribution, with an average particle diameter of 110.4 ± 4.2 nm and 70.8 ± 2.8 nm as revealed by NTA and DLS, respectively (**Fig. 1 A**); and a round morphology as shown by AFM imaging (**Fig. 1 D**).

PTX was incorporated into exosomes using three methods: a) incubation at room temperature (RT), b) electroporation, and c) mild sonication. The obtained exoPTX formulations were purified from the non-incorporated drug by size-exclusion chromatography and analyzed by HPLC to determine the loading capacity (LC). The typical HPLC profiles for PTX extracted from exosomes (**B**) and PTX standards (**A**) are shown on **Supplemental Fig. 1**. The amount of PTX loaded into exosomes increased as follows: incubation at RT < electroporation << sonication (**Fig. 1A**). Interestingly, DLS studies revealed that the size of exoPTX nanoformulations increased similarly, with the smaller being exoPTX nanoparticles obtained by electroporation or incubation at RT, and the larger being exosomes loaded with PTX by sonication (**Fig. 1A**). These data were confirmed by NTA analysis. Exosomes sonicated in the absence of PTX were even larger than those sonicated with PTX (**Fig. 1A**). We hypothesized this may be due to the stabilization of exosomal membranes by the incorporated drug. We suggested that a reorganization of exosomal membranes under sonication may enable PTX diffusion across relatively tight lipid bilayers. Indeed, fluorescence polarization measurements revealed significant decreases (more than two times) in membrane microviscosity upon sonication (**Fig. 1C**). To address a concern about possible loosing of exosome-bound proteins, we examined the levels of Alix, TSG101, and Flotillin in exosomes before and after sonication using western blot technique (**Fig. 1B**). The data indicate that the mild sonication utilized for PTX loading with six cycles, and intermediate time out for cooling down and restoration, did not significantly affect the protein content of exosomes. It is known that the anionic phospholipid phosphatidylserine is abundant on cell membranes and contributes to the surface charge of individual cellular membranes. To this end, all loading procedures did not significantly alter the zeta potential of the nanocarriers (**Fig. 1A**), suggesting that there were also no major alterations of the lipid content of exosomal membranes. Finally, a complete restoration of membrane microviscosity was observed after a one hour incubation at 37C following sonication procedure (**Fig. 1C**). Retention of shape and round morphology of exosomes (**Fig. 1D**) confirmed this hypothesis.

Next, exoPTX showed burst release within the first three hours, and then displayed a sustained release profile thereafter (**Fig. 1E**). The high stability of exosomes in an aqueous

solution was demonstrated at three temperatures: 4°C, RT, and 37°C over a period of one month (**Supplemental Fig. 2**). Overall, the mild sonication procedure provided the highest amount of drug loading; the obtained LC of 28.29 ± 1.38% (**Fig. 1A**) was much higher than the LC of commercially available formulations of PTX, Taxol (~1% LC), or Abraxane (~10% LC). Therefore, exoPTX obtained by sonication was selected for further experiments.

Accumulation and therapeutic efficacy of exoPTX in target cancer cells *in vitro*

The ability to deliver the drug payload into target cells was studied with fluorescently-labeled exosomes in 3LL-M27 cells, and compared to the commonly used nanocarriers, liposomes and polystyrene nanoparticles (NPs) (37) with the same size and level of fluorescence (**Fig. 2**). Liposomes were prepared by a reverse phase evaporation method as described previously (29). Confocal images revealed a profound accumulation of exosomes in cancer cells and limited uptake of liposomes and NPs (**Fig. 2A**). This result was further confirmed and quantitated in accumulation studies (**Fig. 2B**). Exosomes were taken up about 30 times better than the synthetic nanoparticles, suggesting that PTX loaded into exosomes can be efficiently delivered to cancer cells in therapeutically sufficient quantities. These results clearly show the advantages of exosome-based drug delivery systems over common synthetic nanocarriers and confirmed our previous report regarding the profound accumulation of exosomes in neuronal PC12 cells (29).

The anticancer effects of exoPTX were evaluated in a resistant MDR cells expressing the drug efflux transporter, Pgp ($MDCK_{MDR1}$), and their sensitive counterparts ($MDCK_{WT}$). The loading of PTX into exosomes significantly increased drug cytotoxicity as compared to PTX alone, or Taxol in both sensitive $MDCK_{WT}$ and resistant $MDCK_{MDR1}$ cancer cells (**Table 1**). These results are consistent with earlier reports regarding increased cytotoxicity of another anticancer agent, Dox in cancer cells (23). The most intriguing observation was made, when the effects of various PTX formulations were compared in sensitive and resistant cancer cells. For this purpose, the increased cytotoxicity of the drug was expressed in the form of a “Resistance Reversion Index” (*RRI*), *i.e.* ratio of IC_{50} of PTX alone, and in nanoformulation (e.g. $IC_{50,PTX}/IC_{50,\text{exoPTX}}$, or $IC_{50,PTX}/IC_{50,\text{taxol}}$). Both PTX formulations caused significant sensitization of MDR cells with respect to PTX (**Table 1).** In particular, *RRI* for exoPTX in $MDCK_{MDR1}$ and $MDCK_{WT}$ was 53.33 and 18.38, respectively. In contrast, *RRI* for Taxol in both resistant and sensitive cancer cells was *c.a.* 6 (**Table 1).** Noteworthy, empty sonicated exosomes did not show any cytotoxicity in all studied cell lines (**Supplemental Fig. 3**). Thus, the increase in PTX cytotoxicity afforded by exoPTX was greater in Pgp-overexpressing cells than their sensitive counterparts (**Table 1**).

Mechanistic studies of exoPTX cytotoxic effects

We hypothesized that exoPTX may alter drug intracellular trafficking and bypass the drug efflux system more efficiently than Taxol (in particular, exoPTX may facilitate endosomal release of PTX from exosomes in cancer cells). To prove this hypothesis, we examined the accumulation levels of a fluorescent probe and Pgp substrate, Dox, incorporated into exosomes (exoDox) in $MDCK_{MDR1}$ and $MDCK_{WT}$ cells. First, elevated Pgp expression levels in $MDCK_{MDR1}$ cells, and low, if any, Pgp levels in $MDCK_{WT}$ cells were confirmed by western blot (**Fig. 3A**). Next, the uptake of free Dox and exosome-incorporated drug,

exoDox, was compared in the presence/absence of a Pgp inhibitor, verapamil. As expected, the incorporation of Dox into exosomes significantly increased drug accumulation levels in both sensitive and resistant cancer cells (**Fig. 3B**). Inhibition of Pgp-mediated drug efflux by verapamil increased accumulation of free Dox in resistant $MDCK_{MDR1}$ cells, but did not alter drug accumulation in their sensitive counterparts. Remarkably, verapamil treatment did not affect exoDox accumulation in resistant $MDCK_{MDR1}$ cells, indicating that drug incorporation into exosomes allowed it to bypass this resistance mechanism (**Fig. 3B**).

We demonstrated earlier that the incorporation of Pgp substrates, such as R123 or Dox, into block-copolymer-based nanocarriers, *i.e.* Pluronic micelles, increased drug accumulation in resistant cancer cells due to the inhibition of Pgp efflux transporter by Pluronic macromolecules incorporated into the membranes of resistant cancer cells (28, 38-40). To exclude the possibility that exosomes may inhibit Pgp-mediated efflux by their fusion with cellular membranes, accumulation of R123 in both resistant and sensitive MDCK cancer cells was assessed. R123 does not incorporate into exosomes upon incubation at RT, as was confirmed in our preliminary studies (**Supplemental Fig. 4**). For this purpose, $MDCK_{WT}$ and $MDCK_{MDR1}$ cell monolayers were pretreated with a Pgp inhibitor, verapamil (positive control), or empty exosomes, or media (negative control), and then were treated with R123 solutions for two hours (**Supplemental Fig. 5**). R123 accumulation levels in resistant $MDCK_{MDR1}$ cells were increased almost five times in verapamil pre-treated cells. In contrast, treatment with empty exosomes did not affect R123 accumulation in $MDCK_{MDR1}$ cells (**Supplemental Fig. 5**). As expected, neither treatment with verapamil, nor with empty exosomes, altered R123 accumulation levels in sensitive $MDCK_{WT}$ cells. This indicates that exosomes themselves do not appear to have any inhibitory effect on Pgp-mediated efflux; they allow incorporated drugs to bypass the Pgp efflux protein perhaps, through endocytosis-mediated transport and/or fusion with plasma membranes.

Co-localization of Airway-delivered Exosomes with Pulmonary Metastases in Lewis Lung Carcinoma (LLC) mouse model

To establish an *in vivo* model of pulmonary metastases, C57BL/6 mice were injected intra-tail vein (5×10^6 cells/100 μL) with 3LL-M27 cells. Important, this model is particularly relevant to the present investigation, as it was demonstrated that 3LL-M27 tumor cells have high expression levels of the MDR1 gene and Pgp expression *in vivo* (32). Twenty days later, mice were sacrificed, perfused, and lungs were isolated, sectioned, and stained with Hematoxylin and Eosin (H&E). Multiple metastases were detected in whole lungs (**Supplemental Fig. 6A**). Histological evaluations revealed that the structure of alveoli in tumor-bearing lungs was disrupted by tumor cells (**Supplemental Fig. 6B**). Next, mice were injected with 8FlmC-FLuc-3LL-M27 (red, **Fig. 4**) intra-tail vein as described in Materials and Methods section. 22 days later, autologous exosomes stained with a fluorescent dye, DiD (green), were *i.n.* administered to mice with pulmonary metastases. Four hours later, mice were sacrificed, perfused; lungs were sectioned on microtome and examined by confocal microscopy. Nuclei were stained with DAPI (blue, **Fig. 4**). Confocal images revealed 97.9 ± 2.0% of exosomes were co-localized with lung metastases (**Fig.4**), indicating efficient targeting of exoPTX *in vivo.* A similar experiment was performed with exoDox formulation in order to visualize drug delivery to pulmonary metastases

(**Supplemental Fig. 7**). Non-labeled exosomes loaded with Dox (green, **Supplemental Fig. 7B**) were *i.n.* administered to mice with established 8FlmC-FLuc-3LL-M27 metastases (red, **Supplemental Fig. 7A**). Confocal images revealed a substantial amount of DOX in the lungs co-localized with cancer cells (yellow, **Supplemental Fig. 7C**). These results indicate that airway-administered exosomes reached pulmonary metastases and delivered their drug payload to target cancer cells.

PTX-loaded exosomes produce strong antineoplastic effect in mice with lung metastases

To provide insight into the potential of exosome-based therapeutic delivery, the antineoplastic effects of exoPTX were evaluated in an LLC mouse model. For this purpose, C57BL/6 mice were *i.v.* injected with 8FlmC-FLuc-3LL-M27 cells as described above. 48 hours later, mice were *i.n.* administered exoPTX (10^7 particles/10 μl × 2,), or Taxol, or saline as a control every other day totally, seven times. The progression of pulmonary metastases in treated mice was monitored using IVIS by observing the luminescence of transduced cancer cells in living animals (**Fig. 5A**). Representative images of dorsal planes of the injected animals at day 22 are shown on (**Fig. 5A**). A significant ($p < 0.05$) inhibition of metastases growth by exoPTX treatment was demonstrated (**Fig. 5C**). Taxol treatment was shown to inhibit metastases growth as compared to non-treated controls (saline), although to a lesser extent than exoPTX treatment. At the end point of the experiment (day 22), the lung sections were visualized using confocal microscopy (**Fig. 5B**). A marked number of fluorescent transduced cancer cells (red) were detected in the lungs of animals treated with Taxol (**Fig. 5C**), while only a few cancer cells were observed in the lungs of exoPTX treated animals. Noteworthy, sonicated empty exosomes showed no significant inhibition on pulmonary metastases growth (**Fig. 5A, B**). This confirms the superior antineoplastic efficacy of exoPTX as compared to Taxol.

DISCUSSION

Exosomal carriers can provide advantages of both cell-based drug delivery and nanotechnology for efficient drug transport capable of overcoming various biological barriers. However, several limitations need to be addressed before their use in the clinic. One of the difficulties is the efficient loading exosomes with a therapeutic agent without significant changes in the structure and content of exosomal membranes. In the present study, we utilized various methods for PTX incorporation into exosomes: incubation at RT, electroporation, and mild sonication. The mild sonication of exosomes in the presence of PTX provided the greatest loading capacity. PTX, a highly hydrophobic compound is likely to be incorporated into the hydrophobic inner region of the lipid bilayers of exosomes. We hypothesized that the high rigidity of exosomal membranes may be decreased upon sonication and would thus allow for PTX incorporation into lipid bilayers resulting in a high loading capacity. This hypothesis was confirmed by significant decreases in microviscosity of exosomal membranes upon sonication. Nevertheless, we do not exclude a possibility that a considerable amount of PTX may also be adhered to the surface of exosomes that may account for the burst release from exoPTX observed in the first 3-4 hours. It is worth noting that ~30% of loaded drug was still associated with exosomes after one week in an aqueous solution. Importantly, drug located in the inner bilayer of exosomes may also be available

for use: as the exosomal membrane fuses with the cell or endosomal membrane, its intraluminal cargo may be released into the cytosol of a target cell. Next, the aggregation stability of exoPTX formulations is imperative for their use in clinic. We report here that the obtained exoPTX formulation was stable at various conditions for over a month, which confirms previous reports about the long-term stability of exosomes (41). In addition, exosomes may be lyophilized and reconstituted, while retaining their morphology and other characteristics (29). This provides a clinical link for exosome-based drug formulations, suggesting that multiple lots of exoPTX may be prepared and stored prior to treatment.

Exosomes possess an extraordinary ability to interact with and accumulate in target cancer cells. The obtained data indicates exosomes are taken up in considerably greater numbers than liposomes or polystyrene NPs. In addition, the incorporation of PTX into exosomes may not only increase its solubility, but also allow for overcoming of Pgp-mediated drug efflux. We demonstrated here that incorporation of a Pgp substrate, Dox, into exosomes significantly increased drug accumulation in MDR cells as compared to free DOX, or even to Dox in the presence of a Pgp-inhibitor, verapamil. Next, the increase in cytotoxicity afforded by the exosomal formulation of PTX was considerably greater in resistant cells (*RRI* > 53.33) than sensitive cells (*RRI* = 18.35), while Taxol showed almost no difference in resistant (*RRI* > 5.85) *vs.* sensitive cancer cells (*RRI* = 6.17). This effect may be attributed to the difference in route of internalization of exoPTX, as compared to Taxol. Exosomes and micelles, such as those found in Taxol, are taken up by endocytosis, but exosomes have superior uptake due to the presence of adhesion proteins, tetraspanins, integrins, immunoglobulins, proteoglycans, and lectins (42), which are not found on artificial nanoparticles. Furthermore, exosomes consist of cellular membranes that may fuse with the plasma and/or endocytic membranes and deliver their cargo, bypassing Pgp-mediated efflux. Noteworthy, exosomes themselves did not inhibit Pgp, as the pre-treatment with empty exosomes did not increase accumulation of the Pgp substrate, R123, in resistant cancer cells.

Interestingly, it was suggested that the MDR efflux transporters are likely contribute to the production of drug-loaded exosomes during their biogenesis in resistant cancer cells (43). In addition, Pgp may be also involved in the increased drug sequestration in lysosomes and MVB (44). Thus, Pgp associated with the endosomal membrane excretes the internalized drug into the endosomal lumen, where newly formed cancer exosomes are literally incubated with the drug and become “drug-loaded” before being released from the cell. The same effect was reported with PTX in Pgp-overexpressing bone marrow mesenchymal stromal cells (SR4987) (45). We hypothesized that exoPTX accumulated in the MDR cancer cells may bypass not only efflux by Pgp transporter located on plasma membrane, but also avoid accumulation in lysosomes and MVB of cancer cells, and therefore, reduce drug elimination and increase its therapeutic efficacy in resistant tumors. The investigations regarding this hypothesis are underway in our laboratory.

Finally, the therapeutic efficacy of exoPTX formulation against pulmonary metastases was demonstrated in an LLC mouse model. Intriguingly, airway-delivered exosomes showed near complete co-localization with cancer metastases in this model. The results were confirmed by the significant co-localization of Dox incorporated into exosomes with cancer cells. We speculated that macrophage-released exosomes are likely to have specific proteins

on their surface, which might allow for their preferential accumulation in cancer cells. Furthermore, it is known that exosome-mediated cell-to-cell communication is key in the battle between cancer and the immune system (46). Thus, Parolini *et al.* (47) showed that exosome fusion with target cells occurs more efficiently under acidic conditions, implying that exosomes may be taken up preferentially by tumors (which have an acidic microenvironment) rather than the surrounding healthy tissue. Our results show that exoPTX demonstrated superior inhibition of pulmonary metastases growth in LLC mouse model. All three mechanisms mentioned here are likely to have significant impact on exoPTX anticancer activity, *i.e.*: (i) preferential accumulation in cancer cells, (ii) efficient delivery of incorporated cargo into target cancer cells, and (iii) by-passing Pgp-mediated drug efflux in resistant cancer cells. Indeed, further investigations are necessary to uncover this mechanism.

Supplementary Material

Refer to Web version on PubMed Central for supplementary material.

Acknowledgments

This study was supported by the United States National Institutes of Health grants 1RO1 NS057748 and The Carolina Partnership, a strategic partnership between the UNC Eshelman School of Pharmacy and The University Cancer Research Fund through the Lineberger Comprehensive Cancer Center (to EVB), RR021937 (to AVK), and Ministry of Education and Science of Russian Federation grants 11.G34.31.0004, 02.740.11.5232, and RSF-14-13-00731 (both to AVK and NLK).

Abbreviations

ABC	Accelerated Blood Clearance
exoPTX	exosomes loaded with paclitaxel
MDR	multiple drug resistance
LC	loading capacity
PTX	paclitaxel
Pgp	P glycoprotein
PEG	polyethylene glycol
RES	reticuloendothelial system
R123	Rhodamine 123

REFERENCES

1. Gharpure KM, Wu SY, Li C, Lopez-Berestein G, Sood AK. Nanotechnology: Future of Oncotherapy. Clin Cancer Res. 2015; 21(14):3121–30. Epub 2015/07/17. [PubMed: 26180057]
2. Abu Lila AS, Kiwada H, Ishida T. The accelerated blood clearance (ABC) phenomenon: clinical challenge and approaches to manage. J Control Release. 2013; 172(1):38–47. Epub 2013/08/13. [PubMed: 23933235]

3. Hayeshi R, Masimirembwa C, Mukanganyama S, Ungell AL. The potential inhibitory effect of antiparasitic drugs and natural products on P-glycoprotein mediated efflux. Eur J Pharm Sci. 2006; 29(1):70–81. Epub 2006/07/19. [PubMed: 16846720]

4. Bauer KS, Karp JE, Garimella TS, Wu S, Tan M, Ross DD. A phase I and pharmacologic study of idarubicin, cytarabine, etoposide, and the multidrug resistance protein (MDR1/Pgp) inhibitor PSC-833 in patients with refractory leukemia. Leukemia research. 2005; 29(3):263–71. Epub 2005/01/22. [PubMed: 15661261]

5. Simpson RJ, Jensen SS, Lim JW. Proteomic profiling of exosomes: current perspectives. Proteomics. 2008; 8(19):4083–99. Epub 2008/09/10. [PubMed: 18780348]

6. Kalani A, Tyagi A, Tyagi N. Exosomes: mediators of neurodegeneration, neuroprotection and therapeutics. Molecular neurobiology. 2014; 49(1):590–600. Epub 2013/09/04. [PubMed: 23999871]

7. Dong X, Mumper RJ. Nanomedicinal strategies to treat multidrug-resistant tumors: current progress. Nanomedicine (Lond). 2010; 5(4):597–615. Epub 2010/06/10. [PubMed: 20528455]

8. Yang X, Yi C, Luo N, Gong C. Nanomedicine to overcome cancer multidrug resistance. Current drug metabolism. 2014; 15(6):632–49. Epub 2014/09/27. [PubMed: 25255871]

9. Markman JL, Rekechenetskiy A, Holler E, Ljubimova JY. Nanomedicine therapeutic approaches to overcome cancer drug resistance. Adv Drug Deliv Rev. 2013; 65(13-14):1866–79. Epub 2013/10/15. [PubMed: 24120656]

10. Koziara JM, Whisman TR, Tseng MT, Mumper RJ. In-vivo efficacy of novel paclitaxel nanoparticles in paclitaxel-resistant human colorectal tumors. J Control Release. 2006; 112(3): 312–9. Epub 2006/04/22. [PubMed: 16626835]

11. Ratajczak J, Wysoczynski M, Hayek F, Janowska-Wieczorek A, Ratajczak MZ. Membrane-derived microvesicles: important and underappreciated mediators of cell-to-cell communication. Leukemia. 2006; 20(9):1487–95. Epub 2006/06/23. [PubMed: 16791265]

12. Kalani A, Kamat PK, Chaturvedi P, Tyagi SC, Tyagi N. Curcumin-primed exosomes mitigate endothelial cell dysfunction during hyperhomocysteinemia. Life Sci. 2014; 107(1-2):1–7. Epub 2014/05/02. [PubMed: 24780320]

13. Mathivanan S, Ji H, Simpson RJ. Exosomes: extracellular organelles important in intercellular communication. Journal of proteomics. 2010; 73(10):1907–20. Epub 2010/07/06. [PubMed: 20601276]

14. Alvarez-Erviti L, Seow Y, Yin H, Betts C, Lakhal S, Wood MJ. Delivery of siRNA to the mouse brain by systemic injection of targeted exosomes. Nat Biotechnol. 2011; 29(4):341–5. Epub 2011/03/23. [PubMed: 21423189]

15. Wahlgren J, De LKT, Brisslert M, Vaziri Sani F, Telemo E, Sunnerhagen P, et al. Plasma exosomes can deliver exogenous short interfering RNA to monocytes and lymphocytes. Nucleic acids research. 2012; 40(17):e130. Epub 2012/05/24. [PubMed: 22618874]

16. Johnsen KB, Gudbergsson JM, Skov MN, Pilgaard L, Moos T, Duroux M. A comprehensive overview of exosomes as drug delivery vehicles - endogenous nanocarriers for targeted cancer therapy. Biochim Biophys Acta. 2014; 1846(1):75–87. Epub 2014/04/22. [PubMed: 24747178]

17. Shtam TA, Kovalev RA, Varfolomeeva EY, Makarov EM, Kil YV, Filatov MV. Exosomes are natural carriers of exogenous siRNA to human cells in vitro. Cell communication and signaling : CCS. 2013; 11:88. Epub 2013/11/20. [PubMed: 24245560]

18. Pan Q, Ramakrishnaiah V, Henry S, Fouraschen S, de Ruiter PE, Kwekkeboom J, et al. Hepatic cell-to-cell transmission of small silencing RNA can extend the therapeutic reach of RNA interference (RNAi). Gut. 2012; 61(9):1330–9. Epub 2011/12/27. [PubMed: 22198713]

19. Chen L, Charrier A, Zhou Y, Chen R, Yu B, Agarwal K, et al. Epigenetic regulation of connective tissue growth factor by MicroRNA-214 delivery in exosomes from mouse or human hepatic stellate cells. Hepatology. 2014; 59(3):1118–29. Epub 2013/10/15. [PubMed: 24122827]

20. Maguire CA, Balaj L, Sivaraman S, Crommentuijn MH, Ericsson M, Mincheva-Nilsson L, et al. Microvesicle-associated AAV vector as a novel gene delivery system. Mol Ther. 2012; 20(5):960–71. Epub 2012/02/09. [PubMed: 22314290]

21. Sun D, Zhuang X, Xiang X, Liu Y, Zhang S, Liu C, et al. A novel nanoparticle drug delivery system: the anti-inflammatory activity of curcumin is enhanced when encapsulated in exosomes. Mol Ther. 2010; 18(9):1606–14. Epub 2010/06/24. [PubMed: 20571541]
22. Zhuang X, Xiang X, Grizzle W, Sun D, Zhang S, Axtell RC, et al. Treatment of Brain Inflammatory Diseases by Delivering Exosome Encapsulated Anti-inflammatory Drugs From the Nasal Region to the Brain. Mol Ther. 2011; 19(10):1769–79. Epub 2011/09/15. [PubMed: 21915101]
23. Tian Y, Li S, Song J, Ji T, Zhu M, Anderson GJ, et al. A doxorubicin delivery platform using engineered natural membrane vesicle exosomes for targeted tumor therapy. Biomaterials. 2014; 35(7):2383–90. Epub 2013/12/19. [PubMed: 24345736]
24. Thery C, Amigorena S, Raposo G, Clayton A. Isolation and characterization of exosomes from cell culture supernatants and biological fluids. Curr Protoc Cell Biol. 2006:22. Chapter 3:Unit 3. Epub 2008/01/30. [PubMed: 18228490]
25. Thery C, Ostrowski M, Segura E. Membrane vesicles as conveyors of immune responses. Nat Rev Immunol. 2009; 9(8):581–93. Epub 2009/06/06. [PubMed: 19498381]
26. Wiklander OP, Nordin JZ, O'Loughlin A, Gustafsson Y, Corso G, Mager I, et al. Extracellular vesicle in vivo biodistribution is determined by cell source, route of administration and targeting. Journal of extracellular vesicles. 2015; 4:26316. Epub 2015/04/23. [PubMed: 25899407]
27. Pidaparti M, Bostrom B. Comparison of allergic reactions to pegasparaginase given intravenously versus intramuscularly. Pediatric blood & cancer. 2012; 59(3):436–9. Epub 2011/10/25. [PubMed: 22021170]
28. Batrakova EV, Li S, Elmquist WF, Miller DW, Alakhov VY, Kabanov AV. Mechanism of sensitization of MDR cancer cells by Pluronic block copolymers: Selective energy depletion. British journal of cancer. 2001; 85(12):1987–97. [PubMed: 11747344]
29. Haney MJ, Klyachko NL, Zhao Y, Gupta R, Plotnikova EG, He Z, et al. Exosomes as drug delivery vehicles for Parkinson's disease therapy. J Control Release. 2015 Epub 2015/04/04.
30. Laulagnier K, Vincent-Schneider H, Hamdi S, Subra C, Lankar D, Record M. Characterization of exosome subpopulations from RBL-2H3 cells using fluorescent lipids. Blood Cells Mol Dis. 2005; 35(2):116–21. Epub 2005/07/19. [PubMed: 16023874]
31. Boldytev IA, Molotkovskii IG. [A synthesis and properties of new 4,4-difluoro-3a,4a-diaza-s-indacene (BODIPY))-labeled lipids]. Bioorganicheskaia khimiia. 2006; 32(1):87–92. Epub 2006/03/10. [PubMed: 16523725]
32. Batrakova EV, Li S, Brynskikh AM, Sharma AK, Li Y, Boska M, et al. Effects of pluronic and doxorubicin on drug uptake, cellular metabolism, apoptosis and tumor inhibition in animal models of MDR cancers. J Control Release. 2010; 143(3):290–301. Epub 2010/01/16. [PubMed: 20074598]
33. Batrakova EV, Kelly DL, Li S, Li Y, Yang Z, Xiao L, et al. Alteration of genomic responses to doxorubicin and prevention of MDR in breast cancer cells by a polymer excipient: pluronic P85. Mol Pharm. 2006; 3(2):113–23. Epub 2006/04/04. [PubMed: 16579640]
34. Ferrari M, Fornasiero M, Isetta A. MTT colorimetric assay for testing macrophage cytotoxic activity in vitro. J Immunol Methods. 1990; 131(2):165–72. [PubMed: 2391427]
35. Sena-Esteves M, Tebbets JC, Steffens S, Crombleholme T, Flake AW. Optimized large-scale production of high titer lentivirus vector pseudotypes. Journal of virological methods. 2004; 122(2):131–9. Epub 2004/11/16. [PubMed: 15542136]
36. Brynskikh AM, Zhao Y, Mosley RL, Li S, Boska MD, Klyachko NL, et al. Macrophage delivery of therapeutic nanozymes in a murine model of Parkinson's disease. Nanomedicine (Lond). 2010; 5(3):379–96. Epub 2010/04/17. [PubMed: 20394532]
37. De Jong WH, Borm PJ. Drug delivery and nanoparticles:applications and hazards. Int J Nanomedicine. 2008; 3(2):133–49. Epub 2008/08/09. [PubMed: 18686775]
38. Batrakova E, Lee S, Li S, Venne A, Alakhov V, Kabanov A. Fundamental relationships between the composition of pluronic block copolymers and their hypersensitization effect in MDR cancer cells. Pharmaceutical Research. 1999; 16(9):1373–9. [PubMed: 10496652]

39. Batrakova E, Li S, Alakhov V, Miller D, Kabanov A. Optimal structure requirements for pluronic block copolymers in modifying P-glycoprotein drug efflux transporter activity in bovine brain microvessel endothelial cells. J Pharmacol Exp Ther. 2003; 304(2):845–54. [PubMed: 12538842]
40. Batrakova EV, Li S, Alakhov VY, Elmquist WF, Miller DW, Kabanov AV. Sensitization of Cells Overexpressing Multidrug-Resistant Proteins by Pluronic P85. Pharmaceutical Research. 2003; 20(10):1581–90. [PubMed: 14620511]
41. Kalra H, Adda CG, Liem M, Ang CS, Mechler A, Simpson RJ, et al. Comparative proteomics evaluation of plasma exosome isolation techniques and assessment of the stability of exosomes in normal human blood plasma. Proteomics. 2013; 13(22):3354–64. Epub 2013/10/12. [PubMed: 24115447]
42. Mulcahy LA, Pink RC, Carter DR. Routes and mechanisms of extracellular vesicle uptake. Journal of extracellular vesicles. 2014:3. Epub 2014/08/22.
43. Safaei R, Larson BJ, Cheng TC, Gibson MA, Otani S, Naerdemann W, et al. Abnormal lysosomal trafficking and enhanced exosomal export of cisplatin in drug-resistant human ovarian carcinoma cells. Molecular cancer therapeutics. 2005; 4(10):1595–604. Epub 2005/10/18. [PubMed: 16227410]
44. Yamagishi T, Sahni S, Sharp DM, Arvind A, Jansson PJ, Richardson DR. P-glycoprotein mediates drug resistance via a novel mechanism involving lysosomal sequestration. J Biol Chem. 2013; 288(44):31761–71. Epub 2013/09/26. [PubMed: 24062304]
45. Pascucci L, Cocce V, Bonomi A, Ami D, Ceccarelli P, Ciusani E, et al. Paclitaxel is incorporated by mesenchymal stromal cells and released in exosomes that inhibit in vitro tumor growth: a new approach for drug delivery. J Control Release. 2014; 192:262–70. Epub 2014/08/02. [PubMed: 25084218]
46. Finn OJ. Immuno-oncology: understanding the function and dysfunction of the immune system in cancer. Annals of oncology : official journal of the European Society for Medical Oncology / ESMO. 2012; 23(Suppl 8):viii6–9. Epub 2012/08/29. [PubMed: 22918931]
47. Parolini I, Federici C, Raggi C, Lugini L, Palleschi S, De Milito A, et al. Microenvironmental pH is a key factor for exosome traffic in tumor cells. J Biol Chem. 2009; 284(49):34211–22. Epub 2009/10/06. [PubMed: 19801663]

A

Sample/Method	Size by NTA (nm)	Z-Average size (nm)	Zeta Potential (mV)	Loading Capacity (%)
Naive	110.2 ± 3.3	70.8 ± 2.8	-10.74 ± 1.13	n/a
Incubation	178.7 ± 5.8 (*)	132.2 ± 2.3 (*)	-9.33 ± .44	1.44 ± 0.38
Electroporation	159.0 ± 3.6 (*)	145.3 ± 1.0 (*)	-8.47 ± .55	5.3 ± 0.48
Sonication	217.9 ± 10.1 (*)	287.7 ± 0.7 (*)	-14.07 ± 0.94	28.29 ± 1.38
Empty sonicated	326.0 ± 23.5 (*)	356.1 ± 3.5 (*)	-12.33 ± 0.24	n/a

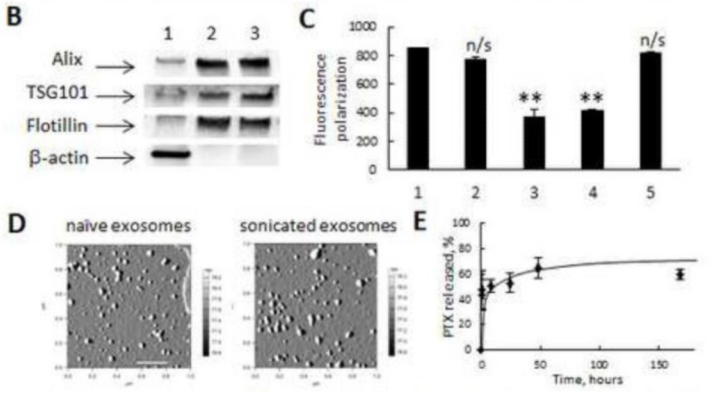

Figure 1. Characterization of PTX exosomal formulations

Exosomes were collected from conditioned media of RAW 264.7 macrophages, and loaded with PTX by various methods: co-incubation at RT; electroporation, and sonication. The size of exoPTX was measured by NTA and DLS (A). The loading with PTX increased the size of exosomes, but did not significantly altered their surface charge. The loading efficiency of exosomes with PTX increased in a row: incubation at RT < electroporation << sonication. The exosome protein content was confirmed by western blot (B). Significant amount of exosome-associated proteins, Alix, TSG101, and Flotillin was detected in naïve (2) and sonicated exosomes (3), but not in the cells (1). Effect of sonication on fluidity of exosomal membranes labeled with BODIPY-PC was examined by fluorescence polarization measurements (C). The microviscosity of exosomal membranes was significantly decreased by six cycles of ultrasound treatment (3) compared to naïve exosomes (1), or exosomes subjected to one sonication cycle (2). The microviscosity of sonicated exosomes was completely restored following one hour incubation period at 37 (5), but not after 30 min incubation (4). The morphology of drug-loaded exosomes was examined by AFM (D). Images revealed small spherical naïve exosomes as well as PTX-loaded exosomes. The bar: 200 nm. A release PTX profile from pre-loaded exosomes was evaluated for the exoPTX formulation obtained by sonication (E). Values are means ± SEM (n = 4). Symbols indicate the relative level of significance compared with naïve exosomes ($p < 0.05$)

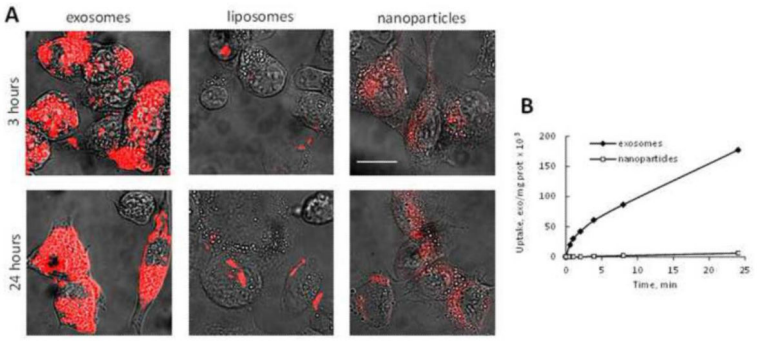

Figure 2. A profound accumulation of exosomes in 3LL-M27 cells *in vitro*

3LL-M27 cells were incubated with fluorescently-labeled (red) exosomes, or liposomes, or PS NPs for various times and the amount of accumulated nanocarriers was examined by confocal microscopy (**A**), and spectrophotometry (**B**). Bar: 10 μm.

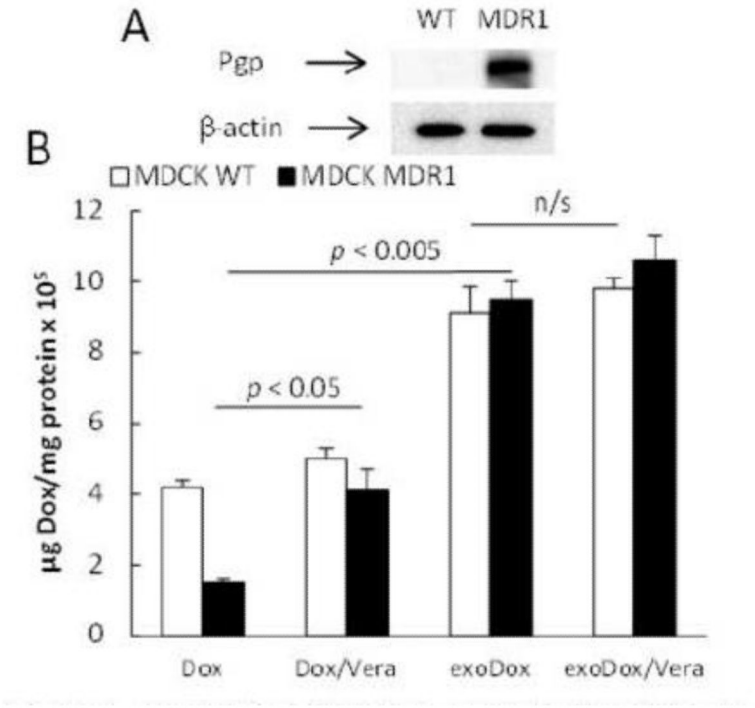

Figure 3. Effect of Pgp inhibition on Dox accumulation in MDR and sensitive cancer cells

The accumulation of free Dox or exoDox in $MDCK_{MDR1}$ and $MDCK_{WT}$ cells was studied in cell lysates. The Dox incorporation into exosomes significantly increased accumulation in sensitive and resistant cells, while no effect of verapamil on exoDOX accumulation was found in both cell lines.

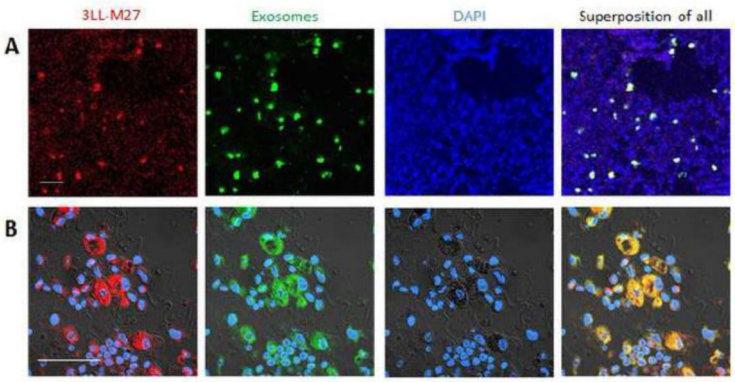

Figure 4. Co-localization of airway-delivered exosomes with pulmonary metastases

Exosomes were isolated from macrophages conditioned media, and labeled with fluorescent dye, DID (green). C57BL/6 mice were *i.v.* injected with 3LL-M27 cells transduced with lentiviral vectors encoding the optical reporter mCherry (8FlmC) fluorescent protein. 21 days later, the mice with established pulmonary metastases (**red**) were *i.n.* injected with DID-labeled exosomes (**green**). 4 hours later, mice were euthanized, perfused, lungs were sectioned, and stained with DAPI (**blue**). The confocal images revealed near complete co-localization of exosomes with metastases (**yellow**). Images were obtained with ×10 (**A**), and ×60 (**B**) magnification. Bar: 50 μm.

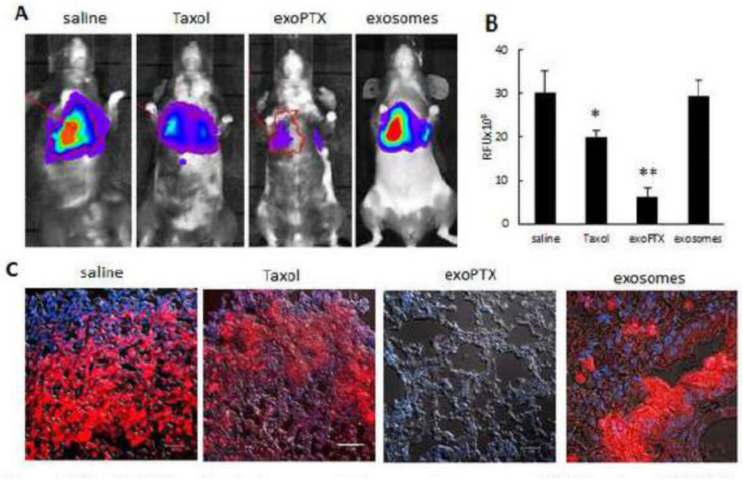

Figure 5. The inhibition of metastases growth in mouse lungs upon exoPTX treatment

C57Bl/6 mice were *i.v.* injected with 8FlmC-FLuc-3LL-M27 (red) cells to establish pulmonary metastases. 48 hour later mice were treated with exoPTX, or Taxol, or saline, or empty sonicated exosomes as a control, and the treatment was repeated every other day, totally seven times. Representative IVIS images were taken at day 21 (A). Statistical significance of metastases levels from IVIS images in lungs of treated animals compared to control mice is shown by asterisk (*$p < 0.05$; **$p < 0.005$) (B). At the endpoint, 21 days later, mice were sacrificed, perfused, and lung slides were examined by confocal microscopy (C). The bar: 10 μm.

Table 1

Cytotoxicity of different PTX formulations in cancer cells. The RRI was calculated as IC_{50} of PTX *vs.* IC_{50} of exoPTX or Taxol

Drug	Cell Line	IC50 (ng/ml)	RRI
exoPTX	3LL-M27	13.57 ± 1.33	9.32
	MDCK wt	23.33 ± 3.77	18.38
	MDCK MDR1	187.5 ± 38.65	>53.33
Taxol	3LL-M27	23.16 ± 1.88	5.46
	MDCK wt	69.54 ± 11.5	6.17
	MDCK MDR1	1708.67 ± 299.93	>5.85
Paclitaxel	3LL-M27	126.41 ± 31.31	1
	MDCK wt	428.77 ± 63.37	1
	MDCK MDR1	>10,000	